

# Structures of the $\alpha$ L I Domain and Its Complex with ICAM-1 Reveal a Shape-Shifting Pathway for Integrin Regulation

Motomu Shimaoka,<sup>1,4</sup> Tsan Xiao,<sup>1,4</sup> Jin-Huan Liu,<sup>2</sup> Yuting Yang,<sup>2</sup> Yicheng Dong,<sup>2,5</sup> Chang-Duk Jun,<sup>1,6</sup> Alison McCormack,<sup>1</sup> Rongguang Zhang,<sup>3</sup> Andrzej Joachimiak,<sup>3</sup> Junichi Takagi,<sup>1</sup> Jia-Huai Wang,<sup>2\*</sup> and Timothy A. Springer<sup>1,\*</sup>

<sup>1</sup>The Center for Blood Research

Department of Pathology

Department of Anesthesia

Department of Pediatrics

<sup>2</sup>Dana-Farber Cancer Institute

Department of Pediatrics

Department of Medicine

Department of Biological Chemistry

Department of Molecular Pharmacology

Harvard Medical School

Boston, Massachusetts 02115

<sup>3</sup>Biosciences Division

Argonne National Laboratory

Argonne, Illinois 60439

## Summary

The structure of the I domain of integrin  $\alpha$ L $\beta$ 2 bound to the Ig superfamily ligand ICAM-1 reveals the open ligand binding conformation and the first example of an integrin-IgSF interface. The I domain  $Mg^{2+}$  directly coordinates Glu-34 of ICAM-1, and a dramatic swing of I domain residue Glu-241 enables a critical salt bridge. Liganded and unliganded structures for both high- and intermediate-affinity mutant I domains reveal that ligand binding can induce conformational change in the  $\alpha$ L I domain and that allosteric signals can convert the closed conformation to intermediate or open conformations without ligand binding. Pulling down on the C-terminal  $\alpha$ 7 helix with introduced disulfide bonds ratchets the  $\beta$ 6- $\alpha$ 7 loop into three different positions in the closed, intermediate, and open conformations, with a progressive increase in affinity.

## Introduction

Integrins are a family of noncovalently associated,  $\alpha\beta$  heterodimeric transmembrane molecules that mediate cell-cell and cell-extracellular matrix adhesion. Lymphocyte function-associated antigen-1 (LFA-1,  $\alpha$ L $\beta$ 2) is an integrin that is critically important in antigen-specific responses and homing by lymphocytes and together with other  $\beta$ 2 integrins in diapedesis by monocytes and neutrophils at inflammatory sites (Gahmberg et al., 1997; Larson and Springer, 1990; Shimaoka et al., 2002).  $\alpha$ L $\beta$ 2 recognizes intercellular adhesion molecules (ICAMs),

members of the Ig superfamily (IgSF) of which ICAM-1 is the most biologically important (Dustin and Springer, 1999). ICAM-1 is highly inducible on antigen-presenting cells and endothelium by cytokines in inflammation.

Although the extracellular domains of  $\alpha$ L and  $\beta$ 2 are each large and structurally complex, the ligand binding site is contained solely within the 180 residue inserted (I) domain of  $\alpha$ L (Shimaoka et al., 2001, 2002). The I domain is important in ligand binding in the 9 of 18 integrin  $\alpha$  subunits in which it is present. Crystal structures of integrin I domains reveal a dinucleotide binding or Rossmann fold, with a central hydrophobic  $\beta$  sheet surrounded by seven amphipathic  $\alpha$  helices (Lee et al., 1995b; Shimaoka et al., 2002). A  $Mg^{2+}$  ion is coordinated at the “top” of the domain in a metal ion-dependent adhesion site (MIDAS).

Integrins trigger “outside-in” signals in response to ligand binding (Giancotti and Ruoslahti, 1999; Schwartz and Ginsberg, 2002). In B and T cell responses,  $\alpha$ L $\beta$ 2 augments proliferation and protects against apoptosis (Koopman et al., 1994; Van Seventer et al., 1990). Ligand binding induces significant structural rearrangements in the I domain of the integrin  $\alpha$ 2 subunit, as seen in a complex with a collagen-like peptide (Emsley et al., 2000). Compared to the unliganded “closed” conformation of the  $\alpha$ 2 I domain, the liganded “open” conformation exhibits a large 10 Å movement of the C-terminal  $\alpha$  helix down the side of the domain, and a rearrangement in metal coordination at the MIDAS. The metal ion is central in the binding site and directly coordinates a Glu residue in the ligand. A similar conformational change has been observed in the  $\alpha$ M I domain; however, in this case it is induced by a ligand-like contact of the metal in the MIDAS with a Glu residue of a neighboring I domain in the crystal lattice (Lee et al., 1995b). By contrast, multiple  $\alpha$ L I domain structures have consistently revealed the unliganded, closed conformation (Kallen et al., 1999; Legge et al., 2000; Qu and Leahy, 1995, 1996).

In the absence of activation,  $\alpha$ L $\beta$ 2 has low affinity for ligand (Dustin and Springer, 1989; Lollo et al., 1993). In inside-out signaling by integrins, signals received by other receptors activate intracellular signaling pathways that impinge on integrin cytoplasmic domains and make the extracellular domain competent for ligand binding on a timescale of less than 1 s (Hughes and Pfaff, 1998; Lollo et al., 1993; Shimaoka et al., 2002). This unique property enables leukocytes to rapidly respond to signals in the environment, such as foreign antigen or chemoattractants, to activate adhesion and direct cell migration. A disulfide bond has been introduced into the  $\alpha$ L I domain to stabilize the predicted open conformation and was found to increase the affinity for ICAM-1 by 10,000-fold (Shimaoka et al., 2001). This strongly supports the idea that conformation regulates affinity; however, whether the open conformation would be stable in the absence of bound ligand has not been established because all open I domain structures determined to date are ligand bound (Emsley et al., 2000; Lee et al., 1995b). Two activation states have been defined functionally for

\*Correspondence: springer@cbr.med.harvard.edu (T.A.S.), jwang@red.dfci.harvard.edu (J.-H.W.)

<sup>4</sup>These authors contributed equally to this work.

<sup>5</sup>Present address: Institute of Biophysics, Academia Sinica, Beijing, 100101, P. R. China.

<sup>6</sup>Present address: Department of Microbiology and Immunology, Wonkwang University Medical School, Chonbuk 570-749, Korea.

Table 1.  $\alpha$ L I Domain Design and Binding to ICAM-1

I Domain	Open C $\beta$ - C $\beta$	Closed Distance (Å)	$k_{on}$ ( $M^{-1}s^{-1} \times 10^{-3}$ )	$k_{off}$ ( $s^{-1}$ )	$K_D$ ( $\mu$ M)	Class
K287C/K294C	3.8	9.1	115 $\pm$ 7	0.014 $\pm$ 0.001	0.15 $\pm$ 0.016	High
E284C/E301C	7.0	12.5	105 $\pm$ 3	0.045 $\pm$ 0.006	0.36 $\pm$ 0.04	High
L161C/F299C	8.1	11.4	133 $\pm$ 10	0.43 $\pm$ 0.07	3.0 $\pm$ 0.44	Inter.
K160C/F299C	7.8	8.0	103 $\pm$ 15	0.77 $\pm$ 0.07	8.4 $\pm$ 2.4	Inter.
L161C/T300C	13.0	14.9	89 $\pm$ 12	0.76 $\pm$ 0.07	9.4 $\pm$ 2.4	Inter.
K160C/T300C	12.8	10.9	3.4 $\pm$ 0.9	1.2 $\pm$ 0.08	450 $\pm$ 210	Low
L289C/K294C	8.0	3.9	2.3 $\pm$ 0.3	3.6 $\pm$ 0.34	1600 $\pm$ 170	Low
Wild-type	N/A	N/A	3.1 $\pm$ 0.1	4.6 $\pm$ 0.36	1500 $\pm$ 200	Low

The distances between wild-type residue C $\beta$  atoms replaced with cysteine in mutants were measured in the open model (Shimaoka et al., 2001) or closed  $\alpha$ L structure (1ZON) (Qu and Leahy, 1996).

The interaction of I domains with immobilized ICAM-1 in the presence of Mg<sup>2+</sup> was monitored with surface plasmon resonance.  $k_{on}$  and  $k_{off}$  were obtained by curve fitting using a 1:1 binding model.  $K_D$  was calculated by Scatchard plot using binding at steady state.

Structures of the underlined mutants K287C/K294C and L161C/F299C are determined here. N/A, not applicable.

$\alpha$ L $\beta$ 2 on cells activated by differing stimuli. Both states are competent for cell adhesion, but high-affinity soluble ligand binding is only detectable for one of these states (Constantin et al., 2000; Stewart et al., 1996; van Kooyk et al., 1999). However, the concept that I domains might exist in intermediate- as well as high-affinity states (Shimaoka et al., 2001) has not been tested by attempting to mutationally stabilize such states or define their structure.

Because of the key role of the interaction between LFA-1 and ICAM-1 in immune responses, defining its structural basis is of great interest. Furthermore, development of pharmaceutical antagonists of this interaction is of great importance for treatment of autoimmune disease (Giblin and Kelly, 2001; Gottlieb et al., 2000). Crystal structures have been determined for IgSF molecules recognized by integrins, i.e., ICAM-1 (Bella et al., 1998; Casanovas et al., 1998), ICAM-2 (Casanovas et al., 1997), VCAM-1, and MAdCAM-1 (Wang and Springer, 1998), but not for IgSF complexes with integrins. Here, the crystal structure of the I domain:ICAM-1 complex reveals an atomic view of an integrin-IgSF ligand interface for the first time. Furthermore, multiple I domain structures reveal an intermediate state in the shape-shifting pathway and show that the I domain can be stabilized in the open conformation in the absence of bound ligand.

## Results and Discussion

### Designed $\alpha$ L I Domains

Previously,  $\alpha$ L residues 289 and 294 or residues 287 and 294 were mutated to cysteine to stabilize the closed, or the predicted open, conformations of the I domain, respectively (Table 1; Shimaoka et al., 2001). We made four further pairs of cysteine substitutions where the C $\beta$ -C $\beta$  distances were predicted to be closer in the open than closed conformation and hence should form disulfides that stabilized the open conformation, and we made one pair of cysteine substitutions where the C $\beta$ -C $\beta$  distances were more favorable for the closed conformation (Table 1). All cysteine substitutions were distant from the MIDAS and ligand binding surface so that direct involvement of the mutated residues in ligand binding could be ruled out. All mutations included one

residue in the C-terminal  $\alpha$ 7 helix. None of the new mutations had C $\beta$ -C $\beta$  distances that were optimal for disulfide formation (3.3 to 4.4 Å); however, one or both residues of each pair were in an  $\alpha$  helix or loop where backbone movements should be allowable that would permit disulfide formation.

Affinity and kinetic measurements using surface plasmon resonance (Shimaoka et al., 2001) showed that the mutant  $\alpha$ L I domains fell into three classes (Table 1). Two mutants with the closest C $\beta$ -C $\beta$  distances in the predicted open conformation, and the greatest increase in C $\beta$ -C $\beta$  distances in the closed conformation, bound to ICAM-1 with high affinity ( $K_D$  of 150 to 360 nM). Three mutants, which also had C $\beta$ -C $\beta$  atoms that were closer in the predicted open than the closed conformation, bound ICAM-1 with intermediate affinity ( $K_D$  of 3 to 9  $\mu$ M). Two mutants which had C $\beta$ -C $\beta$  atoms that were closer in the closed than the predicted open conformation had low affinity ( $K_D$  of 0.5 to 1.6 mM), similar to the  $K_D$  of 1.5 mM of the wild-type I domain. DTT reduction of the disulfides of the mutants of the high- and intermediate-affinity classes reduced their affinity to wild-type levels, and EDTA abolished binding, showing that the interactions were Mg<sup>2+</sup> dependent (data not shown). All of the  $\alpha$ L I domain disulfide bond mutants we have made are described here. It is interesting that the affinities of the mutants cluster into three groups of high, intermediate, and low affinity, because this clustering is consistent with the existence of three distinct conformational states, as shown below. The kinetics of the mutants also cluster. Interestingly, the  $k_{on}$  of the intermediate- and high-affinity mutants are increased by a similar amount (Table 1).

### Four Intermediate- and High-Affinity $\alpha$ L I Domain Crystal Structures

Crystal structures were determined for representative intermediate-affinity (L161C/F299C) and high-affinity (K287C/K294C)  $\alpha$ L I domain mutants (Table 2). Each was determined in two forms. Intermediate-affinity I domain structures were determined in the unliganded state (1.3 Å resolution) or in complex with ICAM-1 (3.3 Å). High-affinity I domain structures were determined in the unliganded state (2.5 Å) or in the "pseudo-liganded" state (2.0 Å), i.e., with a ligand-mimetic lattice contact

Table 2. Statistics of X-Ray Diffraction Data Collection and Structure Refinement

	Intermediate-Affinity I Domain		High-Affinity I Domain	
	Unliganded	+ ICAM-1	Unliganded	Pseudo-liganded
Space group	P2 <sub>1</sub> 2 <sub>1</sub> 2 <sub>1</sub>	P1	C222 <sub>1</sub>	P4 <sub>2</sub> 2 <sub>2</sub>
Unit cell				
a, b, c (Å)	40.4, 57.4, 66.9	46.6, 62.9, 81.5	61.9, 121.3, 54.1	35.6, 35.6, 269.6
α, β, γ (°)	90, 90, 90	95.4, 106.7, 90	90, 90, 90	90, 90, 90
Resolution (Å)	50–1.3	50–3.3	50–2.5	50–2.0
Number of reflections (total/unique)	197,616/35,329	23,330/12,338	41,352/7,271	57,584/10,569
αL residues	128–306	128–306	128–300	128–300
Number of protein/ hetero-atoms	1427/329	5680/172	1388/31	1380/91
Completeness (%)	90.2/47.0 <sup>a</sup>	92.3/70.7 <sup>a</sup>	94.2/60.4 <sup>a</sup>	82.1/67.5 <sup>a</sup>
I/σ(I)	17.8/2.4 <sup>a</sup>	7.7/1.5 <sup>a</sup>	8.4/2.0 <sup>a</sup>	12.6/3.5 <sup>a</sup>
R <sub>merge</sub> (%) <sup>b</sup>	8.8/35.2 <sup>a</sup>	9.4/41.2 <sup>a</sup>	18.4/41.3 <sup>a</sup>	9.4/38.1 <sup>a</sup>
Rmsd bond lengths	0.012 Å	0.016 Å	0.005 Å	0.006 Å
Rmsd bond angles	2.4°	1.7°	1.3°	1.3°
R <sub>work</sub> <sup>c</sup>	15.6%	26.4%	25.0%	21.3%
R <sub>free</sub> <sup>d</sup>	20.0%	31.3%	28.7%	26.5%
Average B factor	15.9 Å <sup>2</sup>	67.3 Å <sup>2</sup>	34.7 Å <sup>2</sup>	23.7 Å <sup>2</sup>
Ramachandran plot (core/disallowed) <sup>e</sup>	91.6%/0%	72.7%/0%	80.5%/0%	90.6%/0%
PDB code	1MJN	1MQ8	1MQA	1MQ9

<sup>a</sup>The second of each pair of numbers corresponds to the last resolution shell.

<sup>b</sup> $R_{\text{merge}} = \sum_h \sum_i |I_i(h) - \langle I(h) \rangle| / \sum_h \sum_i I_i(h)$ , where  $I_i(h)$  and  $\langle I(h) \rangle$  are the  $i^{\text{th}}$  and mean measurement of the intensity of reflection  $h$ .

<sup>c</sup> $R_{\text{work}} = \sum_n |F_{\text{obs}}(h)| - |F_{\text{calc}}(h)| / \sum_n |F_{\text{obs}}(h)|$ , where  $F_{\text{obs}}(h)$  and  $F_{\text{calc}}(h)$  are the observed and calculated structure factors, respectively. No I/σ cutoff was applied.

<sup>d</sup> $R_{\text{free}}$  is the R value obtained for a test set of reflections consisting of a randomly selected 10% (for the unliganded intermediate-affinity, unliganded and pseudo-liganded high-affinity structures) or 5% (the I domain-ICAM-1 complex structure) subset of the data set excluded from refinement.

<sup>e</sup>Residues in core (most favorable) and disallowed regions of the Ramachandran plot as reported by Procheck (Laskowski et al., 1993).

at the MIDAS. All structures were solved using molecular replacement (Table 2).

### Structure of an Integrin—IgSF Complex

A fragment of ICAM-1 containing IgSF domains 1–3 (residues 1–291) crystallized in complex with the intermediate-affinity αL I domain (Figure 1A). There is no meaningful density for IgSF domain 3 of ICAM-1, which appears to be mobile within the crystal lattice. Domains 1 and 2 of ICAM-1 have an extended orientation with an angle between domains 1 and 2 within the range previously observed (Bella et al., 1998; Casasnovas et al., 1998). There are no significant rearrangements in ICAM-1 associated with binding to the αL I domain.

A total of 1250 Å<sup>2</sup> of solvent-accessible surface is buried in the I domain:ICAM-1 contact. This is a small interface for a protein:protein interaction (1600 ± 400 Å<sup>2</sup>) (Conte et al., 1999). A shallow groove bearing the MIDAS on the “top” face of the I domain binds to the side of domain 1 of ICAM-1, making no contacts with the flexible loops at the N-terminal end of domain 1 (Casasnovas et al., 1998) or with domain 2 (Figure 1A). The contacting ICAM-1 β strands lie parallel to the groove (Figure 1A). These are the F and C β strands on the edge of one sheet and the D β strand on the edge of the other sheet. Glu-34 at the end of β strand C of ICAM-1 forms a direct coordination through its acidic side chain to the Mg<sup>2+</sup> ion held in the I domain MIDAS, which is in the open conformation. Glu-34 sits precisely in the middle of the contact surface on ICAM-1 (magenta surface, Figure 2A, top), as does the Mg<sup>2+</sup> ion on the I domain (magenta, Figure 2A, bottom). The contact surface is relatively flat, with the exception that Met-140 on the I domain (Figure

2B, bottom) protrudes and inserts its side chain into a shallow cleft between Met-64 and Pro-36 on ICAM-1 (Figure 2B, top).

The metal coordination bond between the Mg<sup>2+</sup> and Glu-34 is surrounded on the I domain by a ring of hydrophobic residues (Leu-204, Leu-205, and Met-140) and the aliphatic portion of Thr-243 (Figure 2A, bottom). All interacting residues are contributed by the β1-α1, α3-α4, and β4-α5 loops, which also bear metal-coordinating residues and form the MIDAS (Figures 2C and 3A). The ring of hydrophobic residues on the I domain is in contact with a similar ring of hydrophobic residues on ICAM-1 that surround Glu-34: Pro-36, Tyr-66, Met-64, and the aliphatic portions of Gln-62 and Gln-73 (Figure 2A, top). The surrounding nonpolar environment will strengthen the Coulombic interaction between the Glu-34 of ICAM-1 and Mg<sup>2+</sup> of the MIDAS.

Surrounding the hydrophobic ring are polar interactions involving hydrogen bonds and salt bridges that appear to orient ICAM-1 for optimal contact with the I domain and further strengthen their interaction. Many of the hydrogen bonds are backbone to side chain. Hydrogen bonding residues include Thr-35, Pro-36, Asn-68 in ICAM-1, and Gln-143, Thr-243, and His-264 in the I domain (Figure 2C). The overall electrostatic surface of the contact area displays good charge complementarity (Figure 2B). A salt bridge between Glu-241 of the I domain and Lys-39 of ICAM-1, both of which are crucial for ligand binding (Edwards et al., 1998; Fisher et al., 1997), also facilitates positioning of ICAM-1 and the I domain for optimal interaction (Figures 2B and 2C). This contact is only possible because of a dramatic reorientation of the Glu-241 side chain upon conversion of the

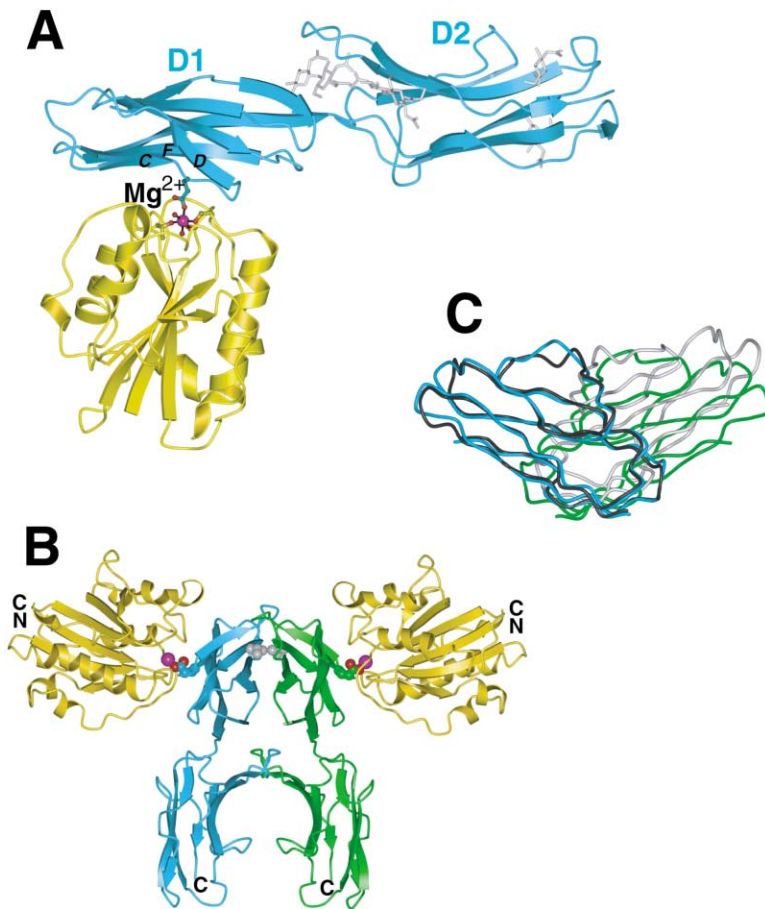


Figure 1. Two  $\alpha$ L I Domains Bound to an ICAM-1 Dimer

(A) Ribbon diagram of one monomeric unit of the intermediate-affinity  $\alpha$ L I domain (gold) complex with ICAM-1 domains 1-2 (cyan). The  $Mg^{2+}$  ion is shown as a magenta sphere. I domain MIDAS and ICAM-1 Glu-34 side chains are shown as ball-and-stick with red oxygen atoms. The interacting  $\beta$  strands C, D, and F of ICAM-1 are labeled. N-acetyl glucosamine residues of ICAM-1 are shown with silver bonds.

(B) The two ICAM-1-I domain complexes in the crystallographic asymmetric unit are shown with the I domains colored gold and the two ICAM-1 molecules colored cyan and green. The 2-fold axis between the ICAM-1 molecules is in the vertical direction, normal to the predicted membrane plane. Positions of the magnesium ions (magenta spheres) and Glu-34 of ICAM-1 (CPK) are shown for reference. The ICAM-1 Val-51 residues at the center of the ICAM-1 dimer interface are shown as gray CPK models.

(C) A view of domains 1 of the ICAM-1 dimer (cyan and green), rotated about  $90^\circ$  from the view in (B), with domain 1 of the uncomplexed ICAM-1 molecule A dimer (Casasnovas et al., 1998) superimposed using domain 1 of one of the ICAM-1 molecules (black), whereas the other one is colored gray. Figures 1-5 are prepared with programs GLR (provided by L. Esser), Molscrip (Kraulis, 1991), Bobscrip (Esnouf, 1997), Raster3D (Merritt and Murphy, 1994), GRASP (Nicholls et al., 1991), and Povray (The Povray Team, <http://www.povray.org>).

$\alpha$ L I domain to the open conformation (Figure 4A), as described below.

Previous mutational studies define the relative importance of the interactions revealed in the interface (Edwards et al., 1998; Fisher et al., 1997; Huang and Springer, 1995; Kamata et al., 1995; Staunton et al., 1990). Glu-34 of ICAM-1 and the residues that coordinate with the  $Mg^{2+}$  in the MIDAS of the I domain have long been identified as crucial. The ICAM-1 contact residues Lys-39, Met-64, Tyr-66, Asn-68, and Gln-73 were also previously recognized as important in mutational studies, as were the I domain contact residues Met-140, Glu-146, Leu-205, Glu-241, Thr-243, and Ser-243.

#### A Dimeric Integrin-Ligand Complex

The crystal asymmetric unit contains two ICAM-1:I domain complexes that are related by 2-fold noncrystallographic symmetry (Figure 1B). The two ICAM-1 molecules dimerize at a hydrophobic interface on the BED sheet of domain 1. A total of  $1100 \text{ \AA}^2$  of solvent-accessible surface is buried. Dimerization at the same hydrophobic interface centered on Val-51 was seen in crystals of ICAM-1 domains 1-2 (Casasnovas et al., 1998) and was suggested to mediate physiologic dimerization on the cell surface. Comparison of ICAM-1 dimers shows some flexibility at the dimer interface (Figure 1C).

The spatial arrangement of the dimeric ICAM-1:I do-

main complex appears ideal for physiologic binding of two  $\alpha$ L $\beta$ 2 heterodimers to a cell surface ICAM-1 dimer. The bottoms of the two I domains bearing the connections to other integrin domains point in opposite directions and away from the connection of ICAM-1 domain 2 to domains 3-5 (Figure 1B). Orienting each half of the dimer similarly in the interface between two adherent cells places the dimer symmetry axis normal to the two cell membranes (Figure 1B). Thus, our structure provides the first glimpse of the orientation between two cells of LFA-1 and ICAM-1 in the immunological synapse (Grakoui et al., 1999). Our structure also provides the first glimpse of a dimeric integrin-ligand interaction. Since essentially all integrin ligands are either dimeric (in solution) or multimeric (on cell surfaces and the extracellular matrix), dimeric interactions of integrins with ligands are likely to be of broad significance.

#### Ligand-Induced Conformational Change in the I Domain: Outside-In Signaling

Comparison between the unliganded and liganded intermediate affinity I domain structures reveals the critical rearrangements in the ligand binding site that are induced by binding to ICAM-1 (see Supplemental Movie S1 at <http://www.cell.com/cgi/content/full/112/1/99/DC1>). The MIDAS of the unliganded intermediate-affinity I domain is in the closed conformation (Figure 3D), with a disposition of coordinating residues and loops identi-

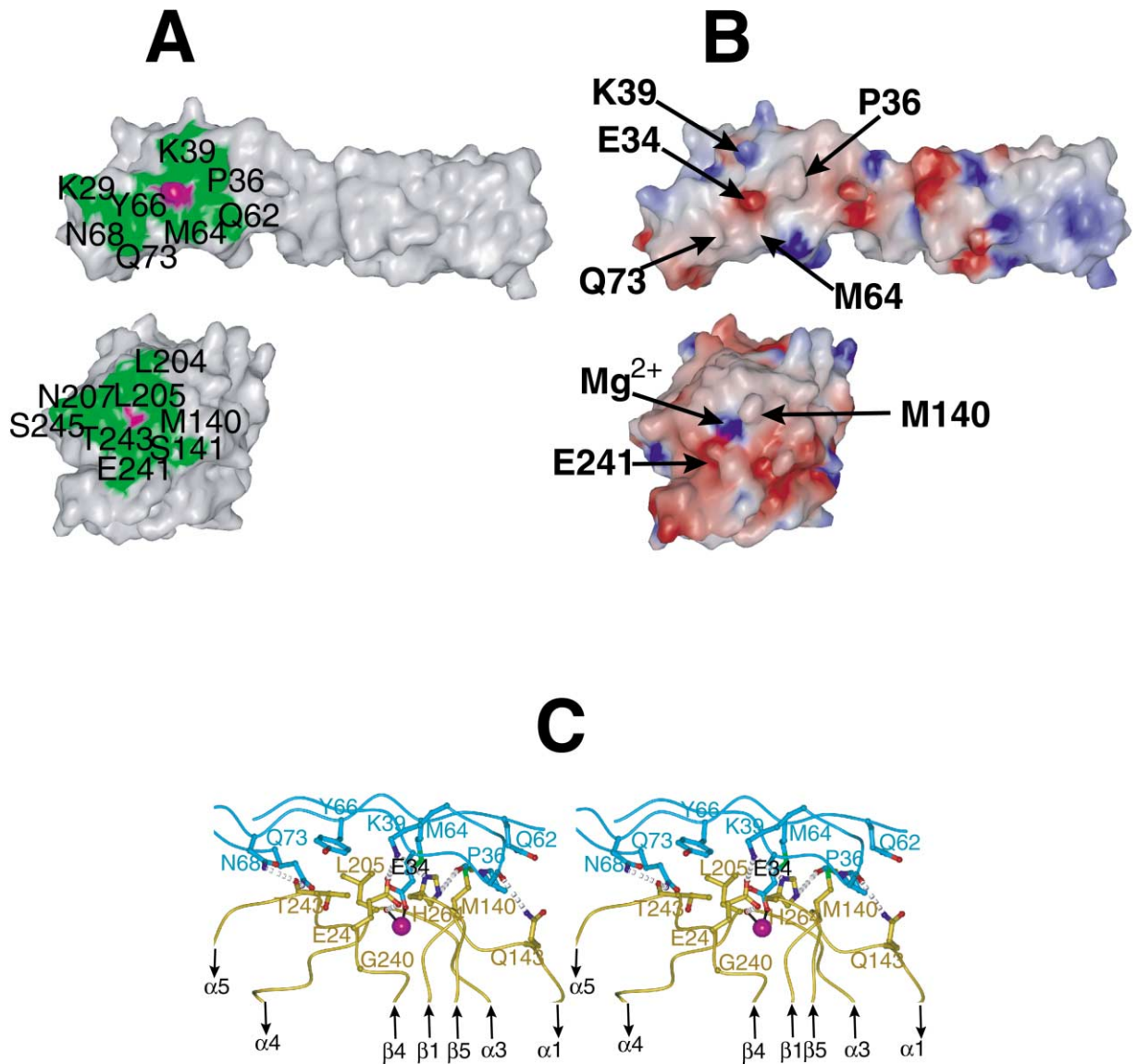


Figure 2. The Interface between the  $\alpha$ L I Domain and ICAM-1

(A) Residues in the I domain:ICAM-1 interface in an open-book representation of the protein surface with the book folded open horizontally, with ICAM-1 above and the I domain below. Interacting residues are colored green and labeled, except for Glu-34 in ICAM-1 and the MIDAS  $Mg^{2+}$  ion in ICAM-1, which are magenta and unlabeled.

(B) The electrostatic surface of the complex in the same open-book representation. The color scale for the charge distribution extends from  $-10 \text{ kT/e}^-$  (red) to  $+10 \text{ kT/e}^-$  (blue) calculated using GRASP (Nicholls et al., 1991). The position of bulges in the interface are marked by arrows, as are the salt-bridged residues Lys-39 in ICAM-1 and Glu-241 in the I domain and Glu-34 in ICAM-1 and the  $Mg^{2+}$  ion in the I domain.

(C) Stereo view of interface details with ICAM-1 in cyan and I domain in gold. The view is about the same as in Figure 1A. The metal ion, oxygens, and nitrogens are represented as magenta, red, and blue spheres, respectively. Metal coordination and hydrogen bonds are represented by solid black lines and gray dotted lines, respectively. Contacting residues are shown as ball-and-stick models. For clarity, MIDAS residues are omitted.

cal to that of the wild-type  $\alpha$ L I domain (Figure 3E). In the open conformation of the MIDAS stabilized by ICAM-1, the direct coordination of I domain residue Asp-239 to the metal is replaced by an indirect coordination mediated by a water molecule, and the metal moves 2 Å toward Thr-206, forming a direct coordination to it (Figure 3A). The change in coordination is linked to a movement in the portion of the  $\beta$ 1- $\alpha$ 1 loop bearing MIDAS residue Ser-141 and the  $\beta$ 4- $\alpha$ 5 loop bearing MIDAS

residue Asp-239 (Figure 4A). The loss of direct metal coordination to Asp-239 not only increases the electrophilicity of the metal for Glu-34 of ICAM-1, but the metal also moves markedly closer to Glu-34 (Figure 4A). The 2 Å movement of Ser-141 enables it to make many contacts with the Glu-34 side chain of ICAM-1 and is associated with a 2.5 Å backbone movement at I domain residue Gln-143 in the  $\beta$ 1- $\alpha$ 1 loop, which brings its side chain into position to hydrogen bond with the backbone of

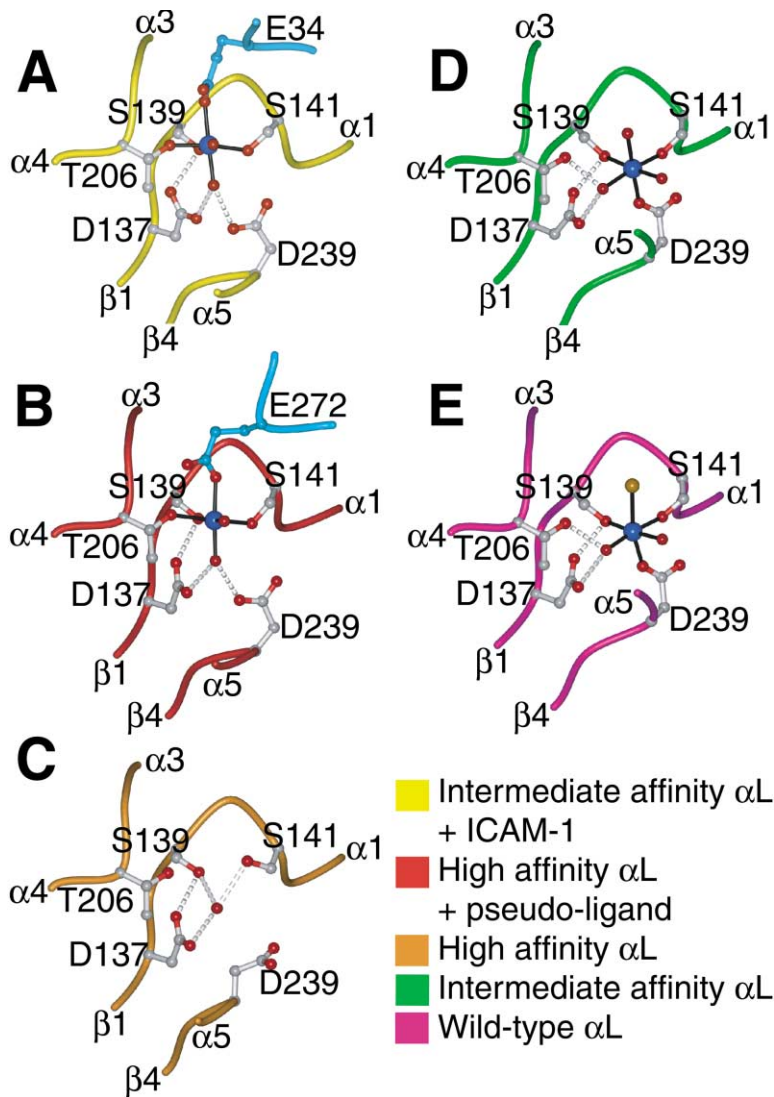


Figure 3. MIDAS Structures

Structures are from the I domain:ICAM-1 complex (A), the pseudo-liganded high-affinity I domain (B), the unliganded high-affinity I domain (C), the unliganded intermediate-affinity I domain (D), and the wild-type I domain (E) (1LFA) (Qu and Leahy, 1996). The keys to the color scheme are shown below, with the ICAM-1 or ligand mimetic molecule colored cyan in (A) and (B). The metal ions are colored blue, water molecule and ligating side chain oxygen atoms are colored red, and the chloride ion from the wild-type I domain structure is colored orange. The MIDAS residues and Glu-34 from ICAM-1 in (A) and Glu-272 from a lattice mate I domain in (B) are shown as ball-and-stick models. Metal coordination and hydrogen bonds are represented by solid black lines and gray dotted lines, respectively.

Pro-36 of ICAM-1 (Figure 2C). The change in coordination of Asp-239 is associated with a dramatic rearrangement in the I domain  $\beta$ 4- $\alpha$ 5 loop bearing this residue (Figure 4A). The loop now bends at Gly-240 away from instead of toward the  $Mg^{2+}$ , with a 4 Å change in  $C_{\alpha}$  position and a backbone flip of Gly-240. The resulting 100° rotation in the side chain of Glu-241 (Figure 4A) brings it into position to form the crucial salt bridge to the side chain of Lys-39 in ICAM-1 (Figure 2C).

The movement of key MIDAS and ligand binding residues in the  $\beta$ 1- $\alpha$ 1 loop “pulls” the entire  $\alpha$ 1 helix toward the center of the domain and is linked to key rearrangements in the hydrophobic core of the I domain (Figure 4A). The side chain of Leu-142 in the  $\beta$ 1- $\alpha$ 1 loop is in contact with Asp-239 and helps “push” it out of direct coordination with  $Mg^{2+}$  and induce the movements in the  $\beta$ 4- $\alpha$ 5 loop at Gly-240 and Glu-241. The side chain of Phe-265 in the  $\beta$ 5- $\alpha$ 6 loop swings away from the  $\beta$ 4- $\alpha$ 5 loop and toward the  $\beta$ 6- $\alpha$ 7 loop to make way for these changes. Previous NMR chemical shift perturbation studies have shown that binding to ICAM-1 induced significant changes at the MIDAS and the

C-terminal region of the  $\alpha$ L I domain (Huth et al., 2000). The changes in the  $\beta$ 1- $\alpha$ 1 and  $\beta$ 4- $\alpha$ 5 MIDAS loops and the inward rigid body movement of the  $\alpha$ 1 helix, which “squeezes” the hydrophobic core of the domain, are essentially identical to those observed in the transition from the closed to open conformation of the  $\alpha$ 2 and  $\alpha$ M I domains (Emsley et al., 2000; Lee et al., 1995a). However, in the absence of ligand binding, the  $\beta$ 6- $\alpha$ 7 loop in the intermediate-affinity I domain is already in a conformation that is intermediate between its open and closed conformations (see below). Upon ligand binding, some readjustments occur in this loop and in  $\beta$ 6 and  $\alpha$ 7, but the  $\beta$ 6- $\alpha$ 7 loop does not assume the open conformation. This appears to be a consequence of constraints imposed by the Cys-161-Cys-299 disulfide bond. The electron density is poorest in the complex structure nearby this disulfide and in  $\beta$ 6 and  $\alpha$ 7, suggesting structural strain, whereas the density is excellent in all regions of the uncomplexed intermediate  $\alpha$ L I domain.

The interaction between LFA-1 and ICAM-1, described here in atomic detail, is paradigmatic of many other cell adhesive interactions between integrins and

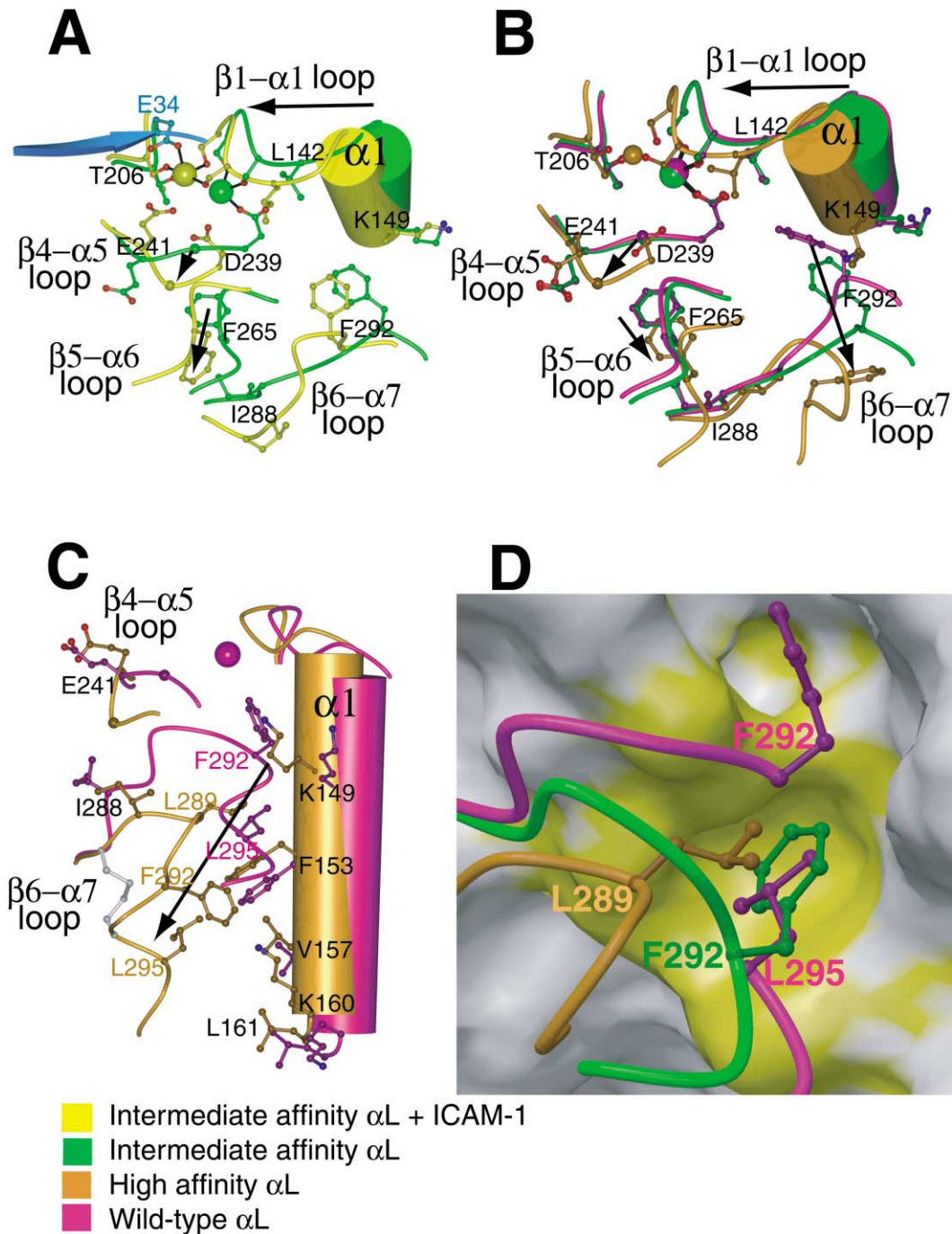


Figure 4. Propagation of Conformational Change in the I Domain

(A–C) The effect of ligand binding (A) and remodeling of the  $\beta 6-\alpha 7$  loop in absence of ligand binding (B and C) are compared on I domain structures near the MIDAS (A and B) and the  $\alpha 7-\alpha 1$  interface (C). Views of (A) and (B) are similar and (C) is approximately orthogonal to (B). Key residues in conformational change are shown in ball-and-stick and labeled, except Gly-240 is unlabeled and shown as a large  $C\alpha$  atom sphere and MIDAS residues Ser-139 and Ser-141 are shown but not labeled. Metal ions are shown as large spheres with the same color as the backbone of the corresponding I domain. The position of the missing metal ion in the unliganded high-affinity structure is simulated by superimposing the metal ion from the pseudo-liganded high-affinity structure and is shown smaller than the other metals. Side chain oxygen atoms are shown as red; water oxygens are omitted for clarity. The directions of major shifts from closed to open conformations are shown with arrows. A portion of ICAM-1 domain-1 containing the metal-coordinating residue E34 is shown in cyan. In (C), the side chain bonds in the designed disulfide bridge (Cys-287-Cys-294) are shown in gray.

(D) The hydrophobic pocket that acts as a detent for the ratchet-like movement of the  $\beta 6-\alpha 7$  loop. The backbone of the  $\beta 6-\alpha 7$  loop and the three residues that occupy the same hydrophobic pocket in the three different conformational states are shown in the same color key as in (A)–(C). The pocket is shown as a GRASP van der Waals surface using the wild-type 1LFA structure with the residues from 287 to the C terminus deleted. The upper hydrophobic pocket is also shown, which is occupied only in the closed conformation (by F292 which is shown in the wild-type structure along with L295). For the closed conformation, the  $\beta 6-\alpha 7$  main chain trace is broken between F292 and L295 for clarity. The view is about the same as in (C). On the otherwise gray GRASP surface, residues Ile-150, Phe-153, Ile-237, Ile-259, and Ile-261 are colored yellow to show the hydrophobic pockets.

IgSF members (Wang and Springer, 1998). The binding site has several remarkable features. Both the shift in coordination at the MIDAS and the remarkable swing of the Glu-241 side chain in the  $\beta 4$ - $\alpha 5$  MIDAS loop appear to be important in switching the I domain into a high-affinity state. Our finding that Glu-241 forms a salt bridge to Lys-39 of ICAM-1 demonstrates a novel mechanism for regulating LFA-1 binding to ICAM-1. This Glu residue is highly conserved, and its swing may be a general mechanism for regulating ligand binding by I domains. Furthermore, the binding interface described here provides an atomic framework for the development of an important class of pharmaceutical antagonists.

Could the wild-type I domain bind in the closed or intermediate conformation to ICAM-1? Superposition on the cocrystal structure shows no significant clashes. The  $\beta 6$ - $\alpha 7$  loop in the closed and intermediate structures is too far from the bound ICAM-1 to block ligand binding. Thus, the downward movement of this loop upon I domain activation has no direct role in exposing the ICAM-1 binding site. In the closed conformation, the  $Mg^{2+}$  ion would be too far away for direct coordination to Glu-34 of ICAM-1, but would be at an appropriate distance for indirect coordination. Therefore, subsequent to ligand binding, reshaping to the open conformation could occur, including lateral movement of the  $\beta 1$ - $\alpha 1$  backbone with readjustments of its side chains that contact ICAM-1. The shifts in MIDAS coordination and the swing of the Glu-241 side chain toward Lys-39 of ICAM-1 could be accommodated subsequent to ICAM-1 binding. Thus, ICAM-1 could bind to an  $\alpha L$  I domain in the closed or intermediate conformation, and then favor a shift to the open conformation.

#### Allosteric Regulation of Ligand Binding by the $\beta 6$ - $\alpha 7$ Loop: Inside-Out Signaling

The high-affinity  $\alpha L$  I domain crystallized in unliganded and pseudo-liganded forms. The two structures have essentially identical open conformations, with a root mean square deviation of 0.57 Å for all  $C\alpha$  atoms. The MIDAS residues of both structures are in the open conformation (Figures 3B and 3C); however, the unliganded high-affinity structure lacks a metal ion at the MIDAS (Figure 3C). In the absence of a metal and a ligand, a water molecule mediates a hydrogen bond network among Asp-137, Ser-139, and Ser-141. The absence of metal coordination and the presence of electrostatic repulsion by Asp-137 cause the side chain of Asp-239 to swing away from other MIDAS residues (Figure 3C). In the pseudo-liganded high-affinity I domain, the metal coordination is completed by an exogenous Glu-272 from a crystallographic symmetry mate (Figure 3B). This lattice contact is similar to that in the open conformation of the  $\alpha M$  I domain (Lee et al., 1995b), except that the Glu is donated by  $\alpha$  helix 6 instead of  $\alpha$  helix 7. The Glu in the ligand-mimetic lattice contact binds in a similar orientation to the Glu in ICAM-1 (Figures 3A and 3B).

The effect of inside-out signaling on I domain conformation is mimicked by pulling down the C-terminal  $\alpha 7$  helix with disulfide bonds in the absence of ligand binding (Figure 5A). In comparison to the wild-type  $\alpha L$  I domain, which assumes the closed conformation (Qu and Leahy, 1995), the  $\beta 6$ - $\alpha 7$  loop of the unliganded interme-

mediate-affinity I domain is partially pulled down, whereas that of the unliganded high-affinity I domain is markedly displaced downward (Figures 4C and 5B). The structures of the  $\alpha M$  and  $\alpha 2$  I domains in the open and closed conformations are shown for comparison (Figure 5B; Emsley et al., 1997, 2000; Lee et al., 1995a, 1995b). The closed  $\alpha L$ ,  $\alpha M$ , and  $\alpha 2$  I domains share an identical conformation of the  $\beta 6$ - $\alpha 7$  loop. The open  $\alpha 2$  and  $\alpha M$  I domain structures also have an identical conformation of the  $\beta 6$ - $\alpha 7$  loop, which differs markedly from the closed conformation of this loop. Importantly, the unliganded, high-affinity  $\alpha L$  I domain mutant has an identical open conformation in the  $\beta 6$  strand and the  $\beta 6$ - $\alpha 7$  loop (Figure 5B). It is these regions that have the important interactions with the hydrophobic core that regulate the conformation of the MIDAS. The conformation of  $\alpha 7$  in the high-affinity  $\alpha L$  mutant differs markedly, partially due to the constraint from the engineered disulfide bond; however, the conformation of  $\alpha 7$  is highly variable, as shown by comparison of different  $\alpha L$  structures in the closed conformation (Figure 5C). Because the remainder of the high-affinity mutant I domain including the MIDAS is in the open, ligand binding configuration, the structural comparison suggests that the conformation of  $\beta$  strand 6 and the  $\beta 6$ - $\alpha 7$  loop, but not the structural details of  $\alpha 7$  per se, are critical for the packing interactions in the hydrophobic core that open the ligand binding site. In intact integrins,  $\alpha 7$  helix movement would therefore appear to be linked to ligand binding only through its effect on  $\beta 6$ - $\alpha 7$  loop conformation.

The  $\beta 6$ - $\alpha 7$  loop of the intermediate-affinity I domain is in a position intermediate between that exhibited in the open and closed conformations of the  $\alpha L$ ,  $\alpha M$ , and  $\alpha 2$  I domains (Figure 5B). In the low-affinity, closed conformation, Phe-292 is in the top of the  $\beta 6$ - $\alpha 7$  loop, buried in a hydrophobic pocket (Figure 4D). The removal of Phe-292 from this pocket is key to enabling rearrangement at the MIDAS (Figures 4B and 4C). Furthermore, another hydrophobic pocket  $\sim 5.5$  Å lower down the side of the domain is occupied successively by Leu-295, Phe-292, and Leu-289 in the low-, intermediate-, and high-affinity structures, respectively (Figure 4D). Although the  $\alpha 7$  helix is disrupted in the high-affinity  $\alpha L$  I domain by the disulfide bond, in the  $\alpha 2$  and  $\alpha M$  I domains the  $\alpha 7$  helix is displaced by two turns of helix down the side of the domain between the open and closed conformations (Emsley et al., 2000; Lee et al., 1995a). In the closed conformation of the  $\alpha L$  I domain, residues 292–295 in the upper part of  $\alpha 7$  form a  $3_{10}$  helix (Qu and Leahy, 1996). In the intermediate conformation of the  $\alpha L$  I domain, this turn of  $3_{10}$  helix beginning with Phe-292 is displaced downward a distance corresponding to one turn of helix, and Phe-292 is deeply buried in the hydrophobic pocket (Figure 4D). The pocket thus acts as a detent that holds the  $\beta 6$ - $\alpha 7$  loop in three different ratchet positions, and each movement displaces the  $\alpha 7$  helix a distance downward corresponding to one turn of helix (see Supplemental Movie S1 at <http://www.cell.com/cgi/content/full/112/1/99/DC1>).

Comparison of the unliganded, high-affinity open structure and the wild-type closed structure shows that the conformational changes induced by pulling down the  $\beta 6$ - $\alpha 7$  loop with a disulfide bridge are first propagated to the hydrophobic core of the I domain and then

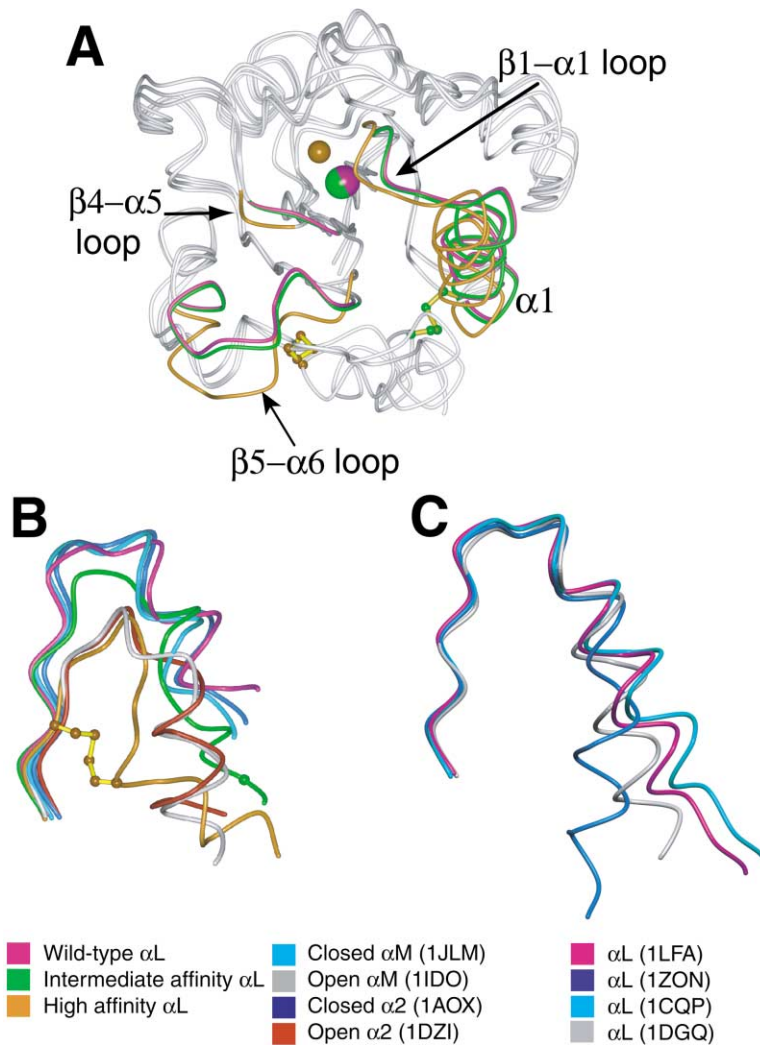


Figure 5. The Structures of the Unliganded Wild-Type, Intermediate-Affinity, and High-Affinity  $\alpha L$  I Domains

(A) The three unliganded  $\alpha L$  I domain backbones are shown superimposed and viewed centered on the MIDAS. Regions of the backbones that differ structurally are labeled and color keyed; other backbone regions are gray. The metal ions at the MIDAS and the atoms in disulfide-linked cysteines are shown in the same colors as the backbone differences; the cysteine side chain bonds are yellow. As in Figure 4B, the position of the missing metal ion in the high-affinity structure is simulated with a smaller sphere.  $\beta 6-\alpha 7$  loop and  $\alpha 7$  are shown in gray for clarity; differences in these regions are shown in (B).

(B) The C-terminal fragments encompassing the  $\beta 6-\alpha 7$  loop for the three unliganded  $\alpha L$  conformations and open and closed  $\alpha 2$  and  $\alpha M$  I domain structures (color keys on bottom left and middle). The side chain bonds of Cys-287 and Cys-294 in the designed disulfide bridge in the high-affinity mutant are shown in yellow; the C $\alpha$  atom of Cys-299 in the designed disulfide of the intermediate mutant is shown as a green sphere.

(C) The C-terminal fragments encompassing the  $\beta 6-\alpha 7$  loop for four different wild-type  $\alpha L$  structures in the closed conformation (color keys on bottom right).

to the MIDAS loops. Pulling down the  $\beta 6-\alpha 7$  loop would have exposed hydrophobic core residues on  $\alpha 1$ ,  $\beta 4$ , and  $\beta 5$ , had there not been nearby structural rearrangements. To shield the hydrophobic core from solvent,  $\alpha 1$  moves  $\sim 2$  Å inward (Figures 4B, 4C, and 5A). In the  $\beta 1-\alpha 1$  loop, the third of three residues that form MIDAS coordinations, Ser-141, shifts 2 Å in backbone position, which in effect changes the metal coordination from the closed to the open conformation. The movement of Leu-142 in the  $\beta 1-\alpha 1$  loop pushes Asp-239 in the  $\beta 4-\alpha 5$  loop from the primary to the secondary metal coordination sphere (Figure 4B). Second, there are concerted downward movements of the  $\beta 5-\alpha 6$  and  $\beta 4-\alpha 5$  loops in order to fill the space left open by the  $\beta 6-\alpha 7$  loop (Figures 4B and 5A). The downward movement of Phe-265 in the  $\beta 5-\alpha 6$  loop allows the flip of the Gly-240 main chain in the  $\beta 4-\alpha 5$  loop. This flip positions the Glu-241 side chain for contact with Lys-39 of ICAM-1 as discussed above. The  $\beta 5-\alpha 6$  loop, which bears Phe-265, possesses high temperature factors and differs significantly among the four structures, largely due to its prominent role in differing crystal lattice contacts. However, residue Phe-265 on this loop is well ordered, and its position appears to be related to the structural transition from the closed

to open conformation (Figure 4A compared to 4B). The conformational changes induced in unliganded structures by downward movement of the  $\beta 6-\alpha 7$  loop (Figure 4B) are identical in all important respects to those induced by ligand binding to the intermediate conformation (Figure 4A), except that after ligation the  $\beta 6-\alpha 7$  loop remains in the intermediate conformation as already discussed.

The unliganded intermediate-affinity and wild-type structures are well superimposable in the regions mentioned above (Figures 4B and 5A). Therefore, pulling down the  $\beta 6-\alpha 7$  loop half-way between the closed and open conformations does not cause significant main chain conformational change elsewhere in the domain and leaves the ligand binding site in the closed conformation (see Supplemental Movie S1 at <http://www.cell.com/cgi/content/full/112/1/99/DC1>). However, this intermediate movement produces an I domain that is energetically primed for the above mentioned structural rearrangements. The key Phe-292 residue in the  $\beta 6-\alpha 7$  loop is already removed from its hydrophobic pocket between  $\beta$  strands 4 and 5 and  $\alpha$  helix 1, and the backbone of the  $\beta 6-\alpha 7$  loop has moved outward, away from the hydrophobic core. Therefore, the lateral movement

of the  $\alpha 1$  helix, the flip of the  $\beta 4$ - $\alpha 5$  loop, and the downward shift of the  $\beta 5$ - $\alpha 6$  loop are achievable with a lower energetic cost, accounting for the increased affinity for ligand.

Our results show that in intact integrins, downward movement of the I domain C-terminal  $\alpha$  helix would be sufficient to convey conformational movements from other domains to the I domain, providing a mechanism for I domain activation in inside-out signaling. The downward movement of the  $\beta 6$ - $\alpha 7$  loop induced here by mutationally introduced disulfide bonds mimics a downward pull thought to be induced in intact integrins by interaction with the neighboring  $\beta$  subunit I-like domain. The idea that the C-terminal  $\alpha 7$  helix and the following linker to the  $\beta$ -propeller domain act as a "bell rope" is supported by findings that mutations in these regions can either activate or inhibit ICAM-1 binding (Alonso et al., 2002; Huth et al., 2000; Luper et al., 2001; Oxvig et al., 1999). The  $\beta 2$  I-like domain regulates ligand binding by the I domain instead of directly participating in ligand binding (Lu et al., 2001), and its MIDAS has been proposed to interact with an acidic residue in the I domain linker to exert the downward pull on the bell rope, which activates ligand binding by the I domain (Alonso et al., 2002; Huth et al., 2000; Lu et al., 2001; Shimaoka et al., 2002).

Our structure of the unliganded high-affinity  $\alpha L$  I domain shows for the first time that the open conformation is stable in the absence of binding to a ligand or pseudo-ligand. Since the disulfide bonds introduced here into isolated I domains mimic a downward pull exerted on the C-terminal  $\alpha$  helix by neighboring domains in intact integrins, our findings suggest that conformational change in I domains could precede ligand binding in intact integrins. This is of considerable biological importance. The on rate for ICAM-1 binding by the closed conformation of the I domain is slow, and the 30-fold increase in  $k_{on}$  observed for the intermediate and open conformations (Table 1) would facilitate the rapid kinetics of integrin-mediated adhesion by leukocytes in the bloodstream, where cellular activation can lead to integrin activation and ligand binding in less than 1 s. Our finding that the open conformation is stable in the absence of ligand binding is supported by studies with activation-sensitive antibodies to the  $\alpha L$  and  $\alpha M$  I domains, which show that changes in I domain conformation occur in intact cell surface integrins upon activation in the absence of ligand binding (Diamond and Springer, 1993; Li et al., 2002; Ma et al., 2002).

Our complex structure and previous crystal studies on  $\alpha M$  and  $\alpha 2$  I domains (Emsley et al., 2000; Lee et al., 1995b) show that ligand binding can also stabilize the open conformation of the I domain. Thus, although it has often been disputed whether conformational change precedes or follows ligand binding, the findings actually support both concepts. Furthermore, the ligand binding site of the unliganded, high-affinity  $\alpha L$  I domain has the same open conformation as the liganded or pseudo-liganded I domains. This demonstrates that signal transmission through the hydrophobic core of the I domain works the same in both directions, i.e., in both inside-out and outside-in signaling.

### An Intermediate Conformation for I Domains

The finding of an intermediate conformational state of the I domain is novel. It is intriguing that there is excellent evidence for two different activation states for  $\alpha L\beta 2$  on cell surfaces (Constantin et al., 2000; Stewart et al., 1996; van Kooyk et al., 1999). Both states are active in binding to ICAM-1 in adhesion assays, whereas only one is sufficiently high affinity to detectably bind soluble ICAM-1. The intermediate conformation of the  $\alpha L$  I domain is very well folded, and indeed the 1.3 Å crystal structure is the highest resolution solved for an I domain to date. The  $\beta 6$ - $\alpha 7$  loop and upper portion of  $\alpha 7$  are very well packed, with an average B factor of 24 Å<sup>2</sup> for all nonhydrogen atoms of residues 288–296. These findings suggest that the intermediate conformation of the  $\beta 6$ - $\alpha 7$  loop represents a discrete conformational state that could exist in intact integrins, and that the intermediate conformation could represent the second active state of  $\alpha L\beta 2$  that is active in cell adhesion but does not bind ligand with high affinity. However, we cannot rule out the possibility that the intermediate conformation of I domains represents a transition state during equilibration of I domains between the open and closed conformations (Shimaoka et al., 2001). A recent study with a fluorescent ligand-mimetic peptide has shown that the  $\alpha 4\beta 1$  integrin exhibits multiple affinity states on the cell surface depending on the activation condition (Chigaev et al., 2001). The presence of multiple affinity states allows more precise regulation of ligand binding and could be essential for the physiological functions of integrins.

The structures of the unliganded intermediate-affinity and high-affinity  $\alpha L$  I domains suggest two discrete steps in a shape-shifting pathway by which inside-out signals can activate integrins for ligand binding. The finding that the affinities of other mutant I domains cluster near those of the I domains with structurally defined open, intermediate, and closed conformations also suggests that these are discrete conformational states in the shape-shifting pathway. Recent averaging of electron microscopic negatively stained images of the extracellular domain of integrin  $\alpha V\beta 3$  suggest that integrins adopt at least three overall conformations: highly bent, extended with a closed headpiece, and extended with an open headpiece (Takagi et al., 2002). It will be very interesting to determine whether integrins that contain I domains also exist in multiple overall shapes and how conformational change in I domains is linked to specific structural alterations elsewhere in integrins.

### Experimental Procedures

#### Protein Expression and Purification

Wild-type and mutant I domains were expressed in *E. coli* BL21 (DE3) (Novagen, Madison, WI), refolded, and purified as described (Legge et al., 2000; Shimaoka et al., 2001), except 0.2 mM CuSO<sub>4</sub> and 1 mM o-phenanthroline were used to catalyze disulfide bond formation and purification was on a monoQ HR5/5 ion-exchange column (Pharmacia) and a Superdex 200 column (Pharmacia). Intramolecular disulfide bonds were confirmed in all mutants by decreased mobility in SDS-PAGE after reduction (Shimaoka et al., 2001).

A cDNA encoding the ICAM-1 signal sequence, residues Q1 to T291, and an additional C-terminal alanine was subcloned into pMT/BiP/V5-His insect cell expression vector (Invitrogen). S2 insect cells (Invitrogen) grown in *Drosophila* serum-free medium (Invitrogen) were cotransfected with 19  $\mu$ g pMT/BiP/V5-His containing the

ICAM-1 fragment and 1  $\mu\text{g}$  pCoHYGRO (Invitrogen) with the calcium phosphate method and selected with 300  $\mu\text{g}/\text{ml}$  hygromycin. Induction with 500  $\mu\text{M}$   $\text{CuSO}_4$  for more than 16 hr yielded 1 mg/l ICAM-1. ICAM-1 was purified as described (Dustin et al., 1992) and further with monoQ ion-exchange chromatography in 20 mM Tris HCl (pH 8) with a gradient of 0 to 1 M NaCl.

#### Surface Plasmon Resonance

Soluble monomeric ICAM-1, or BSA as a negative control, was immobilized on a CM-5 sensor chip by the amine coupling method. I domains were perfused onto the chip in Tris-buffered saline solution plus 1 mM  $\text{MgCl}_2$ , at a flow rate of 10  $\mu\text{l}/\text{min}$ , at 25°C (Shimaoka et al., 2001).

#### Crystallization and Data Collection

Crystals were grown by the hanging drop vapor diffusion method at room temperature. One to two microliters of protein solution (10 to 20 mg/ml) was mixed with an equal volume of well solution on a siliconized glass coverslide and equilibrated against 1 ml of the well solution. The intermediate-affinity I domain was crystallized with 30% PEG 4000, 0.05 M  $\text{MgCl}_2$ , and 0.1 M Tris-Cl (pH 8.5). The intermediate affinity I domain in complex with ICAM-1 domains 1 to 3 was crystallized with 25% PEG-4000 and 0.1 M sodium acetate (pH 4.6). The high-affinity I domain crystallized in two forms. A well solution of 20% PEG 2000 monomethyl ether, 0.025 M  $\text{MnCl}_2$ , and 0.1 M HEPES-Na (pH 7.0) yielded crystals of the pseudo-liganded form. A well solution of 1.2 M ammonium phosphate and 0.1 M Tris-Cl (pH 8.0) yielded crystals of the unliganded form. Crystals were harvested in their mother liquor supplemented with 12%–15% glycerol as cryoprotectant, then flash frozen in liquid nitrogen. Diffraction data were collected at the 19-ID station of the Advanced Photon Source at the Argonne National Laboratory with an SBC2  $3\text{k} \times 3\text{k}$  CCD detector and processed with program suite HKL2000 (Otwinowski and Minor, 1997).

#### Structure Determination and Model Refinement

All four structures were solved using Amore (Navaza, 1994) for molecular replacement and O for visual inspection and model rebuilding (Jones and Kjeldgaard, 1993).

The 1.3 Å structure of the intermediate-affinity I domain was solved using the closed  $\alpha\text{L}$  domain (Qu and Leahy, 1995) as search model. A complete model was built with ARP\_WARP 5.0 (Perrakis et al., 2001). The addition of hydrogen atoms, refinement of multiple side chain conformations, and sulfur atom anisotropy was carried out with SHELX 97\_2 (Sheldrick and Schneider, 1997).

The other three structures at 2.0 to 3.3 Å resolution were refined using CNS version 1.0 protocols for rigid body refinement, positional refinement by Powell minimization, group B factor refinement, and slow-cool simulated annealing molecular dynamics (Brunger et al., 1998). Anisotropic temperature factor correction, bulk solvent correction, and maximum likelihood refinement target were applied throughout.

The structure of the intermediate-affinity I domain ICAM-1 complex was solved using ICAM-1 domains 1 and 2 (Casasnovas et al., 1998) as a search model. The location of the I domain was readily discernible in the electron density map calculated using phases from the ICAM-1 model, and the above intermediate-affinity I domain structure was manually positioned in the map. There are two essentially identical I domain:ICAM-1 complexes in the crystallographic asymmetric unit. Stringent noncrystallographic symmetry (NCS) restraints applied throughout the refinement protocol were monitored by the decrease of  $R_{\text{free}}$ . Specifically, NCS restraints were applied for ICAM-1 domain 1 (except for residues 43–47, which display significant differences in conformation), domain 2, and I domain residues 130–264. The C-terminal part of the I domain was excluded from the NCS restraints due to its flexibility, and this exclusion was monitored by the lowered free R factor. Sigma A weighted  $2F_o - F_c$  and  $F_o - F_c$  maps were computed for visual inspection during rebuilding of the model with O. Analysis of the packing of the molecules in the crystal lattice indicated that domain 3 of ICAM-1 could be accommodated in the lattice. However, the diffuse electron density following domain 2 prohibited modeling domain 3. The final model includes residues 1 to 184 of ICAM-1 and one or two

N-acetylglucosamine residues at each of the four N-linked glycosylation sites. The electron density for I domain residues 285–298 is relatively poor. However, a continuous density that connects the main chain is clearly visible at 0.7 $\sigma$  contour level, with the exception of residues 286 and 287 for both I domains. It appears that these two residues could adopt multiple conformations. Therefore, the Val-286 and Lys-287 side chains are modeled with an occupancy of 0.50 and probably represent the most stable conformation.

The pseudo-liganded high-affinity I domain with a  $\text{Mn}^{2+}$  ion at the MIDAS was solved using the uncomplexed intermediate-affinity I domain structure as a search model. Water molecules with at least one hydrogen bond to protein atoms and a temperature factor below 80 Å<sup>2</sup> were included.

The structure of the unliganded high-affinity I domain was solved using the liganded high-affinity structure as a search model. To minimize model bias, regions of the search model including the three MIDAS loops, the  $\beta 5$ - $\alpha 6$  loop, and the C-terminal fragment starting from  $\beta 6$  were removed during initial cycles of refinement. Simulated annealing omit maps (Hodel et al., 1992) were computed and inspected during model rebuilding. The identity of a water molecule instead of a metal ion at the MIDAS was confirmed by the hydrogen bonding distance (>2.6 Å) as opposed to the magnesium coordinating distance of about 2.0 Å, and the absence of a bipyramidal coordination sphere.

#### Acknowledgments

We would like to thank Rob Meijers for help with ARP\_WARP. This project was supported by NIH grants CA31798 (T.A.S.) and HL48675 (J.-H.W.). T.X. is supported by a postdoctoral fellowship from the Irvington Institute. The calculation of the relative domain orientation of ICAM-1 utilized program HINGE developed by Peter Sun at the NIAID.

Received: July 25, 2002

Revised: November 20, 2002

#### References

- Alonso, J.L., Essafi, M., Xiong, J.P., Stehle, T., and Arnaout, M.A. (2002). Does the integrin  $\alpha\text{A}$  domain act as a ligand for its  $\beta\text{A}$  domain? *Curr. Biol.* 12, R340–R342.
- Bella, J., Kolatkar, P.R., Marlor, C., Greve, J.M., and Rossmann, M.G. (1998). The structure of the two amino-terminal domains of human ICAM-1 suggests how it functions as a rhinovirus receptor and as an LFA-1 integrin ligand. *Proc. Natl. Acad. Sci. USA* 95, 4140–4145.
- Brunger, A.T., Adams, P.D., Clore, G.M., DeLano, W.L., Gros, P., Grosse-Kunstleve, R.W., Jiang, J.-S., Kuszewski, J., Nilges, M., Pannu, N.S., et al. (1998). Crystallography & NMR system: a new software suite for macromolecular structure determination. *Acta Crystallogr. D* 54, 905–921.
- Casasnovas, J.M., Springer, T.A., Liu, J.-h., Harrison, S.C., and Wang, J.-h. (1997). The crystal structure of ICAM-2 reveals a distinctive integrin recognition surface. *Nature* 387, 312–315.
- Casasnovas, J.M., Stehle, T., Liu, J.-h., Wang, J.-h., and Springer, T.A. (1998). A dimeric crystal structure for the N-terminal two domains of ICAM-1. *Proc. Natl. Acad. Sci. USA* 95, 4134–4139.
- Chigaev, A., Blenc, A.M., Braaten, J.V., Kumaraswamy, N., Kepley, C.L., Andrews, R.P., Oliver, J.M., Edwards, B.S., Prossnitz, E.R., Larson, R.S., and Sklar, L.A. (2001). Real-time analysis of the affinity regulation of  $\alpha 4$ -integrin: the physiologically activated receptor is intermediate in affinity between resting and  $\text{Mn}^{2+}$  or antibody activation. *J. Biol. Chem.* 276, 48670–48678.
- Constantin, G., Majeed, M., Giagulli, C., Piccib, L., Kim, J.Y., Butcher, E.C., and Laudanna, C. (2000). Chemokines trigger immediate  $\beta 2$  integrin affinity and mobility changes: differential regulation and roles in lymphocyte arrest under flow. *Immunity* 13, 759–769.
- Conte, L.L., Chothia, C., and Janin, J. (1999). The atomic structure of protein-protein recognition sites. *J. Mol. Biol.* 285, 2177–2198.
- Diamond, M.S., and Springer, T.A. (1993). A subpopulation of Mac-1

- (CD11b/CD18) molecules mediates neutrophil adhesion to ICAM-1 and fibrinogen. *J. Cell Biol.* **120**, 545–556.
- Dustin, M.L., and Springer, T.A. (1989). T cell receptor cross-linking transiently stimulates adhesiveness through LFA-1. *Nature* **341**, 619–624.
- Dustin, M.L., and Springer, T.A. (1999). Intercellular adhesion molecules (ICAMs). In *Guidebook to the Extracellular Matrix and Adhesion Proteins*, T. Kreis and R. Vale, eds. (New York: Sambrook and Tooze).
- Dustin, M.L., Carpen, O., and Springer, T.A. (1992). Regulation of locomotion and cell-cell contact area by the LFA-1 and ICAM-1 adhesion receptors. *J. Immunol.* **148**, 2654–2663.
- Edwards, C.P., Fisher, K.L., Presta, L.G., and Bodary, S.C. (1998). Mapping the intercellular adhesion molecule-1 and -2 binding site on the inserted domain of leukocyte function-associated antigen-1. *J. Biol. Chem.* **273**, 28937–28944.
- Emsley, J., King, S.L., Bergelson, J.M., and Liddington, R.C. (1997). Crystal structure of the I domain from integrin  $\alpha 2\beta 1$ . *J. Biol. Chem.* **272**, 28512–28517.
- Emsley, J., Knight, C.G., Farndale, R.W., Barnes, M.J., and Liddington, R.C. (2000). Structural basis of collagen recognition by integrin  $\alpha 2\beta 1$ . *Cell* **101**, 47–56.
- Esnouf, R.M. (1997). An extensively modified version of MolScript that includes greatly enhanced coloring capabilities. *J. Mol. Graph. Model.* **15**, 132–138.
- Fisher, K.L., Lu, J., Riddle, L., Kim, K.J., Presta, L.G., and Bodary, S.C. (1997). Identification of the binding site in intercellular adhesion molecule 1 for its receptor, leukocyte function-associated antigen 1. *Mol. Biol. Cell* **8**, 501–515.
- Gahmberg, C.G., Tolvanen, M., and Kotovuori, P. (1997). Leukocyte adhesion: structure and function of human leukocyte  $\beta_2$ -integrins and their cellular ligands. *Eur. J. Biochem.* **245**, 215–232.
- Giancotti, F.G., and Ruoslahti, E. (1999). Integrin signaling. *Science* **285**, 1028–1032.
- Giblin, P.A., and Kelly, T.A. (2001). Antagonists of  $\beta 2$  integrin-mediated cell adhesion. *Annu. Rep. Med. Chem.* **36**, 181–190.
- Gottlieb, A., Krueger, J.G., Bright, R., Ling, M., Lebowitz, M., Kang, S., Feldman, S., Spellman, M., Wittkowski, K., Ochs, H.D., et al. (2000). Effects of administration of a single dose of a humanized monoclonal antibody to CD11a on the immunobiology and clinical activity of psoriasis. *J. Am. Acad. Dermatol.* **42**, 428–435.
- Grakoui, A., Bromley, S.K., Sumen, C., Davis, M.M., Shaw, A.S., Allen, P.M., and Dustin, M.L. (1999). The immunological synapse: a molecular machine controlling T cell activation. *Science* **285**, 221–227.
- Hodel, A., Kim, S.-H., and Brunger, A.T. (1992). Model bias in macromolecular crystal structures. *Acta Crystallogr.* **A48**, 851–858.
- Huang, C., and Springer, T.A. (1995). A binding interface on the I domain of lymphocyte function associated antigen-1 (LFA-1) required for specific interaction with intercellular adhesion molecule 1 (ICAM-1). *J. Biol. Chem.* **270**, 19008–19016.
- Hughes, P.E., and Pfaff, M. (1998). Integrin affinity modulation. *Trends Cell Biol.* **8**, 359–364.
- Huth, J.R., Olejniczak, E.T., Mendoza, R., Liang, H., Harris, E.A., Lupher, M.L., Jr., Wilson, A.E., Fesik, S.W., and Staunton, D.E. (2000). NMR and mutagenesis evidence for an I domain allosteric site that regulates lymphocyte function-associated antigen 1 ligand binding. *Proc. Natl. Acad. Sci. USA* **97**, 5231–5236.
- Jones, T.A., and Kjeldgaard, M. (1993). O Version 5.9. (Uppsala, Sweden: Uppsala University).
- Kallen, J., Welzenbach, K., Ramage, P., Geyl, D., Kriwacki, R., Legge, G., Cottens, S., Weitz-Schmidt, G., and Hommel, U. (1999). Structural basis for LFA-1 inhibition upon lovastatin binding to the CD11a I-domain. *J. Mol. Biol.* **292**, 1–9.
- Kamata, T., Wright, R., and Takada, Y. (1995). Critical threonine and aspartic acid residues within the I domains of  $\beta 2$  integrins for interactions with intercellular adhesion molecule 1 (ICAM-1) and C3bi. *J. Biol. Chem.* **270**, 12531–12535.
- Koopman, G., Keehnen, R.M.J., Lindhout, E., Newman, W., Shimizu, Y., Van Seventer, G.A., deGroot, C., and Pals, S.T. (1994). Adhesion through the LFA-1 (CD11a/CD18)-ICAM-1 (CD54) and the VLA-4 (CD49)-VCAM-1 (CD106) pathways prevents apoptosis of germinal center B cells. *J. Immunol.* **152**, 3760–3767.
- Kraulis, P. (1991). MOLSCRIPT: a program to produce both detailed and schematic plots of protein structure. *J. Appl. Crystallogr.* **24**, 946–950.
- Larson, R.S., and Springer, T.A. (1990). Structure and function of leukocyte integrins. *Immunol. Rev.* **114**, 181–217.
- Laskowski, R.A., MacArthur, M.W., Moss, D.S., and Thornton, J.M. (1993). PROCHECK: a program to check the stereochemical quality of protein structures. *J. Appl. Crystallogr.* **26**, 283–291.
- Lee, J.-O., Bankston, L.A., Arnaout, M.A., and Liddington, R.C. (1995a). Two conformations of the integrin A-domain (I-domain): a pathway for activation? *Structure* **3**, 1333–1340.
- Lee, J.-O., Rieu, P., Arnaout, M.A., and Liddington, R. (1995b). Crystal structure of the A domain from the  $\alpha$  subunit of integrin CR3 (CD11b/CD18). *Cell* **80**, 631–638.
- Legge, G.B., Kriwacki, R.W., Chung, J., Hommel, U., Ramage, P., Case, D.A., Dyson, H.J., and Wright, P.E. (2000). NMR solution structure of the inserted domain of human leukocyte function associated antigen-1. *J. Mol. Biol.* **295**, 1251–1264.
- Li, R., Haruta, I., Rieu, P., Sugimori, T., Xiong, J.P., and Arnaout, M.A. (2002). Characterization of a conformationally sensitive murine monoclonal antibody directed to the metal ion-dependent adhesion site face of integrin CD11b. *J. Immunol.* **168**, 1219–1225.
- Lollo, B.A., Chan, K.W.H., Hanson, E.M., Moy, V.T., and Brian, A.A. (1993). Direct evidence for two affinity states for lymphocyte function-associated antigen 1 on activated T cells. *J. Biol. Chem.* **268**, 21693–21700.
- Lu, C., Shimaoka, M., Zang, Q., Takagi, J., and Springer, T.A. (2001). Locking in alternate conformations of the integrin  $\alpha L\beta 2$  I domain with disulfide bonds reveals functional relationships among integrin domains. *Proc. Natl. Acad. Sci. USA* **98**, 2393–2398.
- Lupher, M.L., Jr., Harris, E.A., Beals, C.R., Sui, L., Liddington, R.C., and Staunton, D.E. (2001). Cellular activation of leukocyte function-associated antigen-1 and its affinity are regulated at the I domain allosteric site. *J. Immunol.* **167**, 1431–1439.
- Ma, Q., Shimaoka, M., Lu, C., Jing, H., Carman, C.V., and Springer, T.A. (2002). Activation induced conformational changes in the I domain region of LFA-1. *J. Biol. Chem.* **277**, 10638–10641.
- Merritt, E.A., and Murphy, M.E.P. (1994). Raster 3D version 2.0: a program for photorealistic graphics. *Acta Crystallogr.* **D50**, 869–873.
- Navaza, J. (1994). Amore: an automated package for molecular replacement. *Acta Crystallogr.* **A50**, 157–163.
- Nicholls, A., Sharp, K.A., and Honig, B. (1991). Protein folding and association; insights from the interfacial and thermodynamic properties of hydrocarbons. *Proteins* **11**, 281–296.
- Otwinowski, Z., and Minor, W. (1997). Processing of X-ray diffraction data collected in oscillation mode. *Methods Enzymol.* **276**, 307–326.
- Oxvig, C., Lu, C., and Springer, T.A. (1999). Conformational changes in tertiary structure near the ligand binding site of an integrin I domain. *Proc. Natl. Acad. Sci. USA* **96**, 2215–2220.
- Perrakis, A., Harkiolaki, M., Wilson, K.S., and Lamzin, V.S. (2001). ARP/warp and molecular replacement. *Acta Crystallogr.* **D 57**, 1445–1450.
- Qu, A., and Leahy, D.J. (1995). Crystal structure of the I-domain from the CD11a/CD18 (LFA-1,  $\alpha L\beta 2$ ) integrin. *Proc. Natl. Acad. Sci. USA* **92**, 10277–10281.
- Qu, A., and Leahy, D.J. (1996). The role of the divalent cation in the structure of the I domain from the CD11a/CD18 integrin. *Structure* **4**, 931–942.
- Schwartz, M.A., and Ginsberg, M.H. (2002). Networks and crosstalk: integrin signalling spreads. *Nat. Cell Biol.* **4**, E65–E68.
- Sheldrick, G.M., and Schneider, T.R. (1997). SHELXL: high resolution refinement. In *Methods in Enzymology*, R.M. Sweet and C.W. Carter Jr., eds. (Orlando, FL: Academic Press), pp. 319–343.
- Shimaoka, M., Lu, C., Palframan, R., von Andrian, U.H., Takagi, J.,

and Springer, T.A. (2001). Reversibly locking a protein fold in an active conformation with a disulfide bond: integrin  $\alpha$  L I domains with high affinity and antagonist activity in vivo. *Proc. Natl. Acad. Sci. USA* **98**, 6009–6014.

Shimaoka, M., Takagi, J., and Springer, T.A. (2002). Conformational regulation of integrin structure and function. *Annu. Rev. Biophys. Biomol. Struct.* **31**, 485–516.

Staunton, D.E., Dustin, M.L., Erickson, H.P., and Springer, T.A. (1990). The arrangement of the immunoglobulin-like domains of ICAM-1 and the binding sites for LFA-1 and rhinovirus. *Cell* **61**, 243–254.

Stewart, M.P., Cabanas, C., and Hogg, N. (1996). T cell adhesion to intercellular adhesion molecule-1 (ICAM-1) is controlled by cell spreading and the activation of integrin LFA-1. *J. Immunol.* **156**, 1810–1817.

Takagi, J., Petre, B.M., Walz, T., and Springer, T.A. (2002). Global conformational rearrangements in integrin extracellular domains in outside-in and inside-out signaling. *Cell* **110**, 599–611.

van Kooyk, Y., van Vliet, S.J., and Figdor, C.G. (1999). The actin cytoskeleton regulates LFA-1 ligand binding through avidity rather than affinity changes. *J. Biol. Chem.* **274**, 26869–26877.

Van Seventer, G.A., Shimizu, Y., Horgan, K.J., and Shaw, S. (1990). The LFA-1 ligand ICAM-1 provides an important costimulatory signal for T cell receptor-mediated activation of resting T cells. *J. Immunol.* **144**, 4579–4586.

Wang, J.-h., and Springer, T.A. (1998). Structural specializations of immunoglobulin superfamily members for adhesion to integrins and viruses. *Immunol. Rev.* **163**, 197–215.